

A New $\Sigma - D$ Relation and Its Application to the Galactic Supernova Remnant Distribution

Gary L. Case and Dipen Bhattacharya
 Institute of Geophysics and Planetary Physics, University of California, Riverside, CA 92521;
 case@tigre.ucr.edu, dipen@tigre.ucr.edu

ABSTRACT

Technological advances in radio telescopes and X-ray instruments over the last 20 years have greatly increased the number of known supernova remnants (SNRs) and led to a better determination of their properties. In particular, more SNRs now have reasonably determined distances. However, many of these distances were determined kinematically using old rotation curves (based on $R_{\odot} = 10$ kpc and $V_{\odot} = 250$ km/s). A more modern rotation curve (based on $R_{\odot} = 8.5$ kpc and $V_{\odot} = 220$ km/s) is used to verify or recalculate the distances to these remnants. We use a sample of 36 shell SNRs (37 including Cas A) with known distances to derive a new radio surface brightness-to-diameter ($\Sigma - D$) relation. The slopes derived here ($\beta = -2.64$ including Cas A, $\beta = -2.38$ without Cas A) are significantly flatter than those derived in previous studies. An independent test of the accuracy of the $\Sigma - D$ relation was performed by using the extragalactic SNRs in the Large and Small Magellanic Clouds. The limitations of the $\Sigma - D$ relation and the assumptions necessary for its use are discussed. A revised Galactic distribution of SNRs is presented based on the revised distances as well as those calculated from this $\Sigma - D$ relation. A scaling method is employed to compensate for observational selection effects by computing scale factors based on individual telescope survey sensitivities, angular resolutions and sky coverage. The radial distribution of the surface density of shell SNRs, corrected for selection effects, is presented and compared to previous works.

Subject headings: supernova remnants — Galaxy: structure

1. Introduction

Determining the distances to the Galactic supernova remnants (SNRs) is a difficult but important task. The in-depth study of the remnants has depended largely on observations in the radio regime. However, radio telescope surveys searching for SNRs are biased by three selection effects: i) overlooking SNRs due to their low surface brightness, especially in a region of higher background, ii) failure to detect SNRs due to their small angular size and iii) an absence of uniform coverage of the sky (see also Green 1991). Recent observations of SNRs have been performed with radio telescopes with better sensitivities, higher angular resolutions and more complete sky coverage than the previous generations, as well as with space-based X-ray telescopes. The use of these new instruments has led to the discovery of new SNRs with lower surface brightnesses and smaller angular sizes, resulting in a significant increase in the number of known SNRs. It has also led to a better determination of the physical and observational properties of known remnants. However, most SNRs still do not have well determined distances.

Conventionally, SNRs are classified into three basic types: shell remnants, characterized by diffuse, shell-like emission with steep radio spectra; plerionic or filled-center remnants, containing a central source

with a flat radio spectrum but no shell structure; and composite remnants, which show signs of both a central source and a diffuse shell structure. Distances to the SNRs can be inferred from positional coincidences with H I, H II, and molecular clouds, OB associations or pulsars or from measuring optical velocities and proper motions. Where there is no direct distance determination, estimates can be made for shell remnants by utilizing the radio surface brightness to diameter relationship ($\Sigma - D$) (i. e. Clark & Caswell 1976; Milne 1979; Sakhibov & Smirnov 1982). The mean surface brightness at a specific radio frequency, Σ_ν , is a distance independent parameter and, to a first approximation, is an intrinsic property of the SNR (Shklovsky 1960). If this relationship is given by

$$\Sigma_\nu = AD^\beta, \quad (1)$$

the distance d will be proportional to $\Sigma_\nu^{1/\beta}\theta^{-1}$, or, in terms of observable quantities, $d \propto S_\nu^{1/\beta}\theta^{-(1+2/\beta)}$, where S_ν is the flux density at the observing frequency ν and θ is the angular diameter of the remnant. Composite SNRs may be characterized by a similar relation, but only a few have known distances, and hence a reasonable $\Sigma - D$ relation is difficult to calculate for them.

There exists considerable skepticism about using the $\Sigma - D$ relation to obtain distance estimates (e.g. Green 1984, 1991). Green (1984) pointed out two significant problems with the $\Sigma - D$ relation. First, many of the independently determined distances have a degree of uncertainty. H I absorption measurements can be difficult to interpret and often give reliably only lower distance limits. Associations of SNRs with other objects such as molecular clouds, H I emission regions and OB associations cannot always be made with great confidence. Second, studies of SNRs in the Large Magellanic Cloud, which are all at approximately the same known distance, have shown a spread in intrinsic properties (see discussion in Green 1984). This suggests that for a given surface brightness, there may be a spread in linear diameters, making a unique distance estimate to individual remnants difficult and uncertain. This spread in intrinsic properties likely results from the variety of different environments into which the remnants are evolving. The density and structure of the ambient medium and the lingering effects of the SNR progenitor star could all potentially effect the remnant’s evolution (Allakhverdiyev et al. 1983a, 1983b). However, in SNR samples which are thought to be observationally complete, there is a clear trend for the surface brightness of SNRs to decrease with increasing linear diameter. By using a large number of distance ‘calibrators’ with distance measurements as reliable as possible, a $\Sigma - D$ relation can be constructed and distance estimates can be made to shell remnants for which there is no other distance information available. However, investigators who use distances to individual SNRs based upon the $\Sigma - D$ relation must be aware of the inherent uncertainties and assumptions of this method.

The impetus for this work arose from a need to determine the radial Galactic SNR distribution. The $\Sigma - D$ relation was the only means by which distances could be obtained for most of the known shell SNRs. However, it became apparent that the $\Sigma - D$ relations most often quoted for distance estimates (e.g. Clark & Caswell 1976; Milne 1979) needed to be updated in light of the new information available for SNRs. We show that even with the uncertainties involved in estimating distances to *individual* SNRs, it is possible to use the $\Sigma - D$ relation for examining *ensemble* properties of the SNRs, such as the total number and their radial distribution. In this paper, revised distances are given for all SNRs in Green’s SNR Catalogue (Green 1996a) for which previous information is out-dated or new information is available. These kinematic distances were recalculated when necessary using a more modern rotation curve (with $R_\odot = 8.5$ kpc and $V_\odot = 220$ km/s). Other distances were taken from new pulsar-SNR or molecular cloud-SNR associations. A new $\Sigma - D$ relation for shell type SNRs is presented using a sample of 36 ‘calibrators’ (37 including Cas A) and the assumptions and limitations for the use of the $\Sigma - D$ relation are discussed. The surface brightness distribution of the nearby remnants and a Monte Carlo simulation are used to calculate scale factors in an

attempt to compensate for observational selection effects. These results are used to derive the radial SNR surface density distribution in the Galaxy.

2. SNR Distances and the $\Sigma - D$ Relation

The positional coincidences of Galactic SNRs with H I, H II, and molecular clouds, OB associations or pulsars may provide distance estimates to the remnants. However, of the 215 SNRs in Green’s present catalog (August 1996 version), only 64 have independently determined distances (38 of 160 shell type, 5 of 9 filled center, 18 of 31 composite and 3 of 15 unknown type). In this analysis, any shell remnant which has an associated pulsar, regardless of whether or not any kind of radio plerion is observed, is considered a composite. Therefore, the number of shell and composite type SNRs given here differs from the numbers in Green’s Catalogue. Using a number of known diameters (from the shell remnants with established distances) one can derive a $\Sigma - D$ relationship for a given radio frequency. For those shell-type remnants which have no direct distance information, we can then estimate their distances using this relation. Unless stated otherwise, the flux densities and surface brightnesses used in this analysis are referenced to 1 GHz.

Previous $\Sigma - D$ relations have indicated that the power law index β in Eq. 1 lies in the range -2.8 to -4 . Clark & Caswell (1976) used 20 SNRs (14 shell, 2 filled center, 2 composite, 1 of unknown type, 1 no longer regarded as an SNR) as distance calibrators and found $\beta = -3$ in the surface brightness range $2 \times 10^{-20} < \Sigma_{408} < 5 \times 10^{-19} \text{ W m}^{-2} \text{ Hz}^{-1}$ (they suggested $\beta \approx -10$ for $\Sigma_{408} < 2 \times 10^{-20}$). This surface brightness limitation excluded the three brightest remnants including Cas A. They also excluded RCW 103, for which they had what they considered a reliable distance, but was far away from their fit in the $\Sigma - D$ plane. In addition, 9 of the 20 calibrators had only lower limits on the distance, and the lower limit was taken to be the actual distance. Milne (1979) used the 11 SNRs from Clark & Caswell with known distances, added back the four remnants that had been excluded and added 7 more with known distances for a total of 22 SNRs (18 shell, 3 composite, and 1 filled center) and obtained $\beta = -3.8$. Lozinskaya (1981) used 21 of the 22 SNRs (excluding the Crab) in Milne’s list, with revised distances to three of them, and added 5 others whose distances she had determined from optical observations for a total of 26 (22 shell and 4 composite) and found $\beta = -3.45$, roughly half way between the values given by Clark & Caswell and Milne. Sakhibov & Smirnov (1982) used 38 SNRs (including those from Lozinskaya) that they classify as shell-type (but actually includes at least 4 remnants that we classify as composite) out of a larger sample of 57 calibrators of all types to derive $\beta = -3.4 \pm 0.5$, agreeing closely with Lozinskaya and, within their error, with Clark & Caswell and Milne as well. For their larger sample they obtain $\beta = -2.8 \pm 0.4$. Li & Wheeler (1984) have derived the flattest relation for shell SNRs with $\beta = -2.77$. Huang & Thaddeus (1985) attempted to use a more homogeneous subsample consisting of 12 shell SNRs located near large molecular clouds and found $\beta = -3.21$. However, all of these studies used old rotation curves.

Table 1. Shell SNRs with known distances

Catalog name	Other name	Surface Brightness ($\text{W m}^{-2} \text{Hz}^{-1} \text{sr}^{-1}$)	Distance (kpc)	Diameter (pc)	Ref. ^a
G4.5+6.8....	Kepler's SNR	3.2×10^{-19}	4.5	4	1
G13.3-1.3...		^b	3.0	46	2
G18.8+0.3....	Kes 67	2.7×10^{-20}	8.1	32	*
G31.9+0.0....	3C391	1.0×10^{-19}	7.2	12	3,4
G33.6+0.1....	Kes 79	3.3×10^{-20}	7.1	21	*
G43.3-0.2....	W49B	4.8×10^{-19}	7.5	8	*
G46.8-0.3....	HC30	9.5×10^{-21}	6.4	28	*
G49.2-0.7....	W51	2.7×10^{-20}	6.0	52	5
G53.6-2.2....	3C400.2	1.3×10^{-21}	5.0	44	*
G54.4-0.3....	HC40	2.6×10^{-21}	3.3	38	*
G74.0-8.5....	Cygnus Loop	8.6×10^{-22}	0.8	45	6
G78.2+2.1....	γ Cygni	1.4×10^{-20}	1.2	21	7,8
G84.2-0.8....		5.2×10^{-21}	4.5	24	9
G89.0+4.7....	HB21	3.1×10^{-21}	0.8	24	10
G111.7-2.1...	Cas A	1.6×10^{-17}	3.4	5	11
G116.5+1.1..		3.4×10^{-22}	5.0	101	*
G116.9+0.2..	CTB 1	1.2×10^{-21}	3.1	31	12
G119.5+10.2..	CTA 1	6.7×10^{-22}	1.4	37	13
G120.1+1.4..	Tycho's SNR	1.3×10^{-19}	4.5	11	14
G132.7+1.3..	HB3	1.1×10^{-21}	2.2	51	15,16
G156.2+5.7..		6.2×10^{-23}	3.0	96	17,18
G160.9+2.6..	HB9	9.9×10^{-22}	2.2	83	*
G166.0+4.3..	VRO 42.05.01	5.5×10^{-22}	4.5	57	19
G166.2+2.5..	OA 184	2.6×10^{-22}	4.5	104	19
G189.1+3.0..	IC443	1.2×10^{-20}	1.5	20	20
G205.5+0.5..	Monoceros	5.0×10^{-22}	1.6	102	21
G260.4-3.4...	Puppis A	6.5×10^{-21}	2.2	35	22
G296.5+10.0..	PKS 1209-52	1.2×10^{-21}	1.6	36	23,*
G304.6+0.1..	Kes 17	3.3×10^{-20}	7.9	18	*
G309.8+0.0..		5.4×10^{-21}	3.6	23	7
G315.4-2.3...	RCW 86	4.2×10^{-21}	2.8	34	24
G327.6+14.6..	SN1006	3.2×10^{-21}	2.1	18	25,26
G330.0+15.0..	Lupus Loop	1.6×10^{-21}	1.2	63	27

Table 1—Continued

Catalog name	Other name	Surface Brightness ($\text{W m}^{-2} \text{ Hz}^{-1} \text{ sr}^{-1}$)	Distance (kpc)	Diameter (pc)	Ref. ^a
G332.4–0.4...	RCW 103	4.2×10^{-20}	3.4	10	*
G348.5+0.1..	CTB 37A	4.8×10^{-20}	9.0	39	*
G348.7+0.3..	CTB 37B	1.4×10^{-20}	9.0	45	*
G349.7+0.2..		6.0×10^{-19}	13.8	9	*
G359.1-0.5...		3.7×10^{-21}	9.2	64	28

^aDistances to remnants marked with an ‘*’ are recalculated from references in Table 2.

^bG13.3-1.3 is an SNR recently identified in X-rays (by ROSAT), and has not yet had a radio surface brightness published.

References. — (1) Bandiera 1987; (2) Seward et al. 1995; (3) Reynolds & Moffett 1993; (4) Wilner et al. 1998; (5) Koo, Kim & Seward 1995; (6) Minkowski 1958; (7) Huang & Thaddeus 1985; (8) Green 1989b; (9) Feldt & Green 1993; (10) Tatematsu et al. 1990; (11) Reed et al. 1995; (12) Hailey & Craig 1994; (13) Pineault et al. 1993; (14) Schwarz et al. 1995; (15) Routledge et al. 1991; (16) Normandeau et al. 1997; (17) Reich, Fürst & Arnal 1992; (18) Pfeffermann, Aschenbach & Predehl 1991; (19) Landecker et al. 1989; (20) Fesen 1984; (21) Odegard 1986; (22) Reynoso et al. 1995; (23) Roger et al. 1988; (24) Rosado et al. 1996; (25) Long, Blair & van den Bergh 1988; (26) Winkler et al. 1997; (27) Leahy, Nousek & Hamilton 1991; (28) Uchida et al. 1992

We have searched the literature to find recent and accurate distances to as many shell remnants as possible. Many of the remnants have more than one distance available. For these remnants, we have either chosen the most recent measurement, or used an average of the available estimates (if the distance range is narrow). Our sample of 37 shell remnants with published distances, which is used to derive the $\Sigma - D$ relation, is listed in Table 1. Only the references for the distances actually used are given in the Table. The surface brightnesses and angular diameters (used to calculate the linear diameters) are taken from Green’s Catalogue.

Most of the kinematic distances given in Green’s Catalogue, as well as the distances used by the authors above, were calculated using 10 kpc as the solar distance from the Galactic Center and a solar velocity of 250 km/s. Some of these remnants now have more recently determined distances, where modern rotation curves with $R_{\odot} = 8.5$ kpc and $V_{\odot} = 220$ km/s were employed. For those SNRs that still do not have kinematic distances based on a modern rotation curve, the original references for the distance information were checked in order to obtain the kinematic velocities determined from H I absorption, mean optical velocities or associated CO or H I emission. The distances were then recalculated using the rotation curve given by Burton & Gordon (1978), with corrections by Fich, Blitz & Stark (1989), for the inner Galaxy and a flat rotation curve outside the Solar Circle. Saken et al. (1992) used the modern rotation curve of Clemens (1985), with the modification that a flat curve was used outside 5 kpc, to derive distances to several remnants. However, this is a non-standard rotation curve implementation, as fiducial rotation curves employ a flat curve only outside the Solar Circle. For this reason, the distances derived by Saken et al. are not used in Table 1. In total, kinematic distances for 17 remnants (14 shell, 1 composite, 2 filled-center) were recalculated and are listed in Table 2. Distances to 11 other composite remnants were assigned the distance to their associated pulsars. Those shell remnants in Table 1 which had kinematic distances recalculated have an ‘*’ in the reference column.

For distances to the other shell remnants in Table 1, two were obtained from an association of the SNR with an H II region and an OB association (G189.1+3.0, G205.5+0.5), three from associations with a molecular cloud and an OB association (78.2+2.1, G89.0+4.7, G309.8+0.0), one from optical kinematics and historical observations (G4.5+6.8), three from optical proper motions (G74.0-8.5, G111.7-2.1, G327.6+14.6), one from the modeling of its X-ray emission (G330.0+15.0), one from modelling of its X-ray emission and from associated H I emission (G119.5+10.2), two from X-ray absorption and associated H I emission (G296.5+10.0, G156.2+5.7) and eleven from the literature in which a modern rotation curve had already been used (G31.9+0.0, G49.2-0.7, G84.2-0.8, G116.9+0.2, G120.1+1.4, G132.7+1.3, G166.0+4.3, G166.2+2.5, G260.4-3.4, G315.4-2.3, G351.9-0.5). Note that the distances listed in Table 1 are the revised distances (where relevant).

The diameters derived from the new distances are shown in Figure 1, from which the relation

$$\Sigma_{1\text{GHz}} = 5.43_{-3.26}^{+8.16} \times 10^{-17} D^{(-2.64 \pm 0.26)} \text{ W m}^{-2} \text{ Hz}^{-1} \text{ sr}^{-1}. \quad (2)$$

is obtained. The typical errors in the kinematic distances are about 10-25%, depending on the resolution and sensitivity of the measurements and the error in the rotation curve parameters. This error does not include uncertainty due to the presence of noncircular motions associated with the object (i.e. CO cloud) or feature (i.e. H I emission), which is hard to quantify. The error in distances derived from the modeling of x-ray emission is typically 30% (Kassim et al. 1994). For distances estimated by associating the remnant with an object such as an OB association, CO cloud or H II region, the distance to the object may be fairly well determined, but the association itself may be less certain, making an error estimate difficult. In these cases, we do not incorporate the SNR into Table 1 unless there is at least one other corroborating distance

Table 2. SNRs with revised distances

Name	Type ^a	Distance (kpc)	Method	Ref.
G5.4-1.2	C?	4.6	Pulsar coincidence	1
G6.4-0.1	C	3.3	Mean optical velocity	2
G8.7-0.1	C? ^b	3.9	Pulsar coincidence	1
G18.8+0.3 . . .	S	8.1	H I absorption	3
G21.5-0.9 . . .	F	6.3	H I absorption	4
G33.6+0.1 . . .	S	7.1	H I absorption	5
G34.7-0.4 . . .	C? ^b	3.3	Pulsar coincidence	1
G43.3-0.2 . . .	S	7.5	H I absorption	6
G46.8-0.3 . . .	S	6.4	H I absorption	7
G53.6-2.2 . . .	S	5.0	optical kinematics	8
G54.4-0.3 . . .	S	3.3	CO association	9
G69.0+2.7 . . .	C? ^b	2.5	Pulsar coincidence	10
G114.3+0.3 . . .	C? ^b	2.5	Pulsar coincidence	1
G116.5+1.1 . . .	S	5.0	H I absorption	11
G130.7+3.1 . . .	F	3.3	H I absorption	12
G160.9+2.6 . . .	S	2.2 ^c	Mean optical velocity	2
G180.0-1.7 . . .	C? ^b	1.5	Pulsar coincidence	10
G296.5+10.0 . . .	S	1.6	associated H I shell	13
G304.6+0.1 . . .	S	7.9	H I absorption	3
G308.8-0.1 . . .	C?	8.7	Pulsar coincidence	1
G320.4-1.2 . . .	C	4.4	Pulsar coincidence	1
G332.4-0.4 . . .	S	3.4	H I absorption	3
G341.2+0.9 . . .	C?	6.9	Pulsar coincidence	1
G343.1-2.3 . . .	C?	1.8	Pulsar coincidence	1
G348.5+0.1 . . .	S	9.0	H I absorption	3
G348.7+0.3 . . .	S	9.0	H I absorption	3
G349.7+0.2 . . .	S	13.8	H I absorption	3
G354.1+0.1 . . .	C?	4.2	Pulsar coincidence	1

^aS - Shell remnant; F - Filled-center remnant; C - Composite remnant.

^bThese SNRs are classified in Green’s catalog as shell or unknown type. They have been classified here as possible composite type because of the association of the remnant with a pulsar.

^cPossible association with a pulsar at 1.8 kpc.

References. — (1) Frail, Goss & Whiteoak 1994; (2) Lozinskaya 1981; (3) Caswell et al. 1975; (4) Davelaar et al. 1986; (5) Frail & Clifton 1989; (6) Radhakrishnan et al. 1972; (7) Sato 1979; (8) Rosado 1983; (9) Junkes, Fürst & Reich 1992; (10) Anderson et al. 1996; (11) Reich & Braunsfurth 1981; (12) Roberts et al. 1993; (13) Dubner et al. 1986

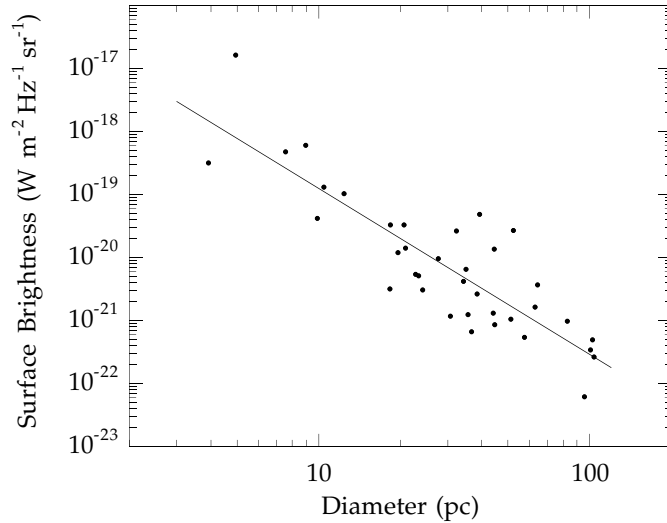


Fig. 1.— The surface brightness versus diameter ($\Sigma - D$) relation for shell SNRs using the distance calibrators in Table 1 (including Cas A).

estimate. Since it is difficult to assign realistic errors to the diameters, equal weighting was used in these $\Sigma - D$ fits.

This $\Sigma - D$ relation is flatter than those obtained in the studies mentioned above. Some used fewer remnants than our study, some used non-shell remnants, and they all used old rotation curves. Radio and X-ray observations made in recent years have had better sensitivities and angular resolutions, which has led to the addition of new shell remnants with lower Σ (with large D) and smaller θ to the current catalogue. Newly determined distances and revised distances using more modern rotation curves have also increased the number of shell remnants that can now be included in the $\Sigma - D$ relation. The outlier point in Fig. 1 is Cas A. We treat this remnant as a special case (see below) and derive a separate $\Sigma - D$ relation without Cas A. If Cas A is excluded, we obtain the relation

$$\Sigma_{1\text{GHz}} = 2.07^{+3.10}_{-1.24} \times 10^{-17} D^{(-2.38 \pm 0.26)} \text{ W m}^{-2} \text{ Hz}^{-1} \text{ sr}^{-1} \quad (3)$$

It is this relation which will be used throughout the remainder of this paper. When the 17 composite remnants with known distances and radio surface brightnesses are added, the relation becomes slightly flatter, with $\beta = -2.21 \pm 0.24$.

Matthewson et al. (1983a) classified SNRs based on their optical features into four categories: oxygen-rich, Balmer-dominated, plerionic-composite and evolved. The emission from the oxygen-rich SNRs arises from shocks interacting more with circumstellar material lost by the progenitor star in the last stages of evolution than with matter swept up from the interstellar medium (ISM), leading van den Bergh (1988a) to suggest that they arose from Type Ib supernova explosions, e.g. the explosion of a massive ($\gtrsim 18 M_{\odot}$) O or Wolf-Rayet star. Van den Bergh (1988a) categorized the Galactic SNRs Cas A, Puppis A and G292.0+1.8 as oxygen-rich SNRs. Among these three, G292.0+1.8 is classified as a composite (Green 1996a) and Puppis A is an older SNR (~ 7000 yrs; van den Bergh 1988a). Cas A is the only young oxygen

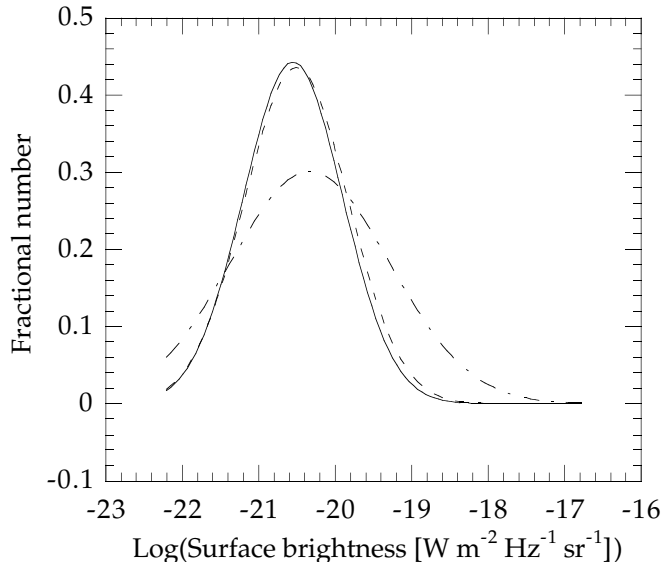


Fig. 2.— The surface brightness distributions for all shell SNRs in Green’s Catalog (solid line), the 20 shell SNRs within 3 kpc of the Sun (dashed line) and the sample of 36 shell SNRs (excluding Cas A) with known distances (dot dashed line). The sample with known distances is biased towards brighter remnants. The distributions are fit to gaussians with a lower cutoff at $\Sigma_c = 5 \times 10^{-23} \text{ W m}^{-2} \text{ Hz}^{-1} \text{ sr}^{-1}$. The distribution for shell SNRs within 3 kpc of the Sun is used to determine scale factors to compensate for observational selection effects (see §4).

rich SNR known in our Galaxy. Its radio surface brightness is ≈ 25 times greater than the next brightest SNR in Table 1. Even the two shell SNRs with ages comparable to Cas A, the remnants of Kepler’s and Tycho’s supernovae, are ≈ 30 and ≈ 100 times fainter, respectively. However, Kepler and Tycho, along with SN1006, are categorized as Balmer dominated remnants (van den Bergh 1988a). The Balmer-dominated remnants have filamentary shells that are strong in the Balmer lines of hydrogen but weak in O III and S II and are powered by a high velocity, nonradiative, collisionless shock encountering the gas of the surrounding ISM. It has been speculated that these remnants arise from Type Ia supernova explosions. Cas A is observed to have a jet-like feature (Kamper & van den Bergh 1976; Fesen, Becker & Blair 1987), something which has not been observed in other shell SNRs. The scatter in the $\Sigma - D$ relation (see Fig. 1) is such that the surface brightness of Cas A lies 3σ off the fit given in Eq. 2. This suggests that young, Cas A-like remnants of Type Ib supernova explosions ought to be treated differently than the other shell SNRs. Puppis A was retained in the fit as it is an older, evolved remnant. If Puppis A is excluded, the slope of the $\Sigma - D$ relation does not change significantly (from $\beta = -2.379$ to $\beta = -2.382$).

The issue of selection effects in the sample used to obtain the $\Sigma - D$ relation must be addressed. Figure 2 shows the fractional number of all shell SNRs as a function of surface brightness (solid line), along with the fractional number of shell SNRs used in obtaining the $\Sigma - D$ relation in this work (dot dashed line). Also shown is the surface brightness distribution for shell SNRs within 3 kpc of the Sun (dashed line). The latter will be used when the selection effects of the entire sample are discussed (see §4). Apparently,

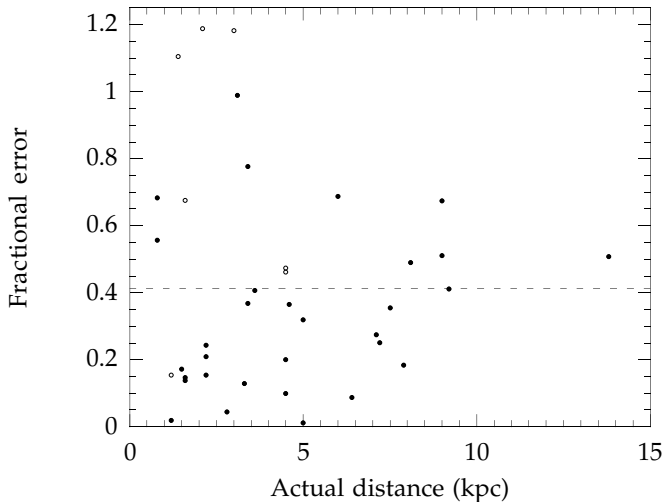


Fig. 3.— The fractional error, f , of the distances derived from our $\Sigma - D$ relation with respect to the actual distances for the shell SNRs given in Table 1, excluding Cas A. The open circles are those shell remnants with $z > 200$ pc. The average fractional error for all of the remnants is 0.41 and is shown by the dashed line.

the sample of shell remnants with known distances (i.e. Table 1) is underrepresented with respect to low surface brightness remnants as compared to the total sample. This can be attributed to the fact that it is easier to determine distances to brighter remnants, whether because they are younger, allowing distances to be obtained from proper motions, or because their higher surface brightnesses allow a clearer interpretation of emission/absorption spectra.

An attempt was made to compensate for this bias by utilizing a weighting function in the fit for the $\Sigma - D$ relation. A weighting function was derived by dividing the Σ -distribution for the complete sample by the Σ -distribution for the SNRs with known distances. This function then would allow the SNRs with lower surface brightness to have more weight in the fit. The slope obtained from the weighted fit is $\beta = -1.68 \pm 0.65$. The weighted fit is not well constrained since a large part of the sample is effectively excluded due to the large errors assigned to the overrepresented part of the Σ -distribution. This has prompted us to use the unweighted fit of Eq. 3 throughout the remainder of this paper. However, it should be noted that as more fainter shell remnants have distances determined, the slope of the $\Sigma - D$ relation may become flatter.

In order to get an estimate of the accuracy of the $\Sigma - D$ relation for individual SNR distances, a fractional error was defined as

$$f = \left| \frac{d_{obs} - d_{sd}}{d_{obs}} \right|, \quad (4)$$

where d_{obs} is the observationally determined distance and d_{sd} is the distance derived from the $\Sigma - D$ relation. The fractional errors for the SNRs used to obtain the $\Sigma - D$ relation are plotted versus the actual distances in Figure 3. The average fractional error is $\bar{f} = 0.41$ and is represented by the dashed line in Fig. 3. The fractional errors are all less than $f = 0.7$ with the exception of SN1006, CTA 1 and G156.2+5.7

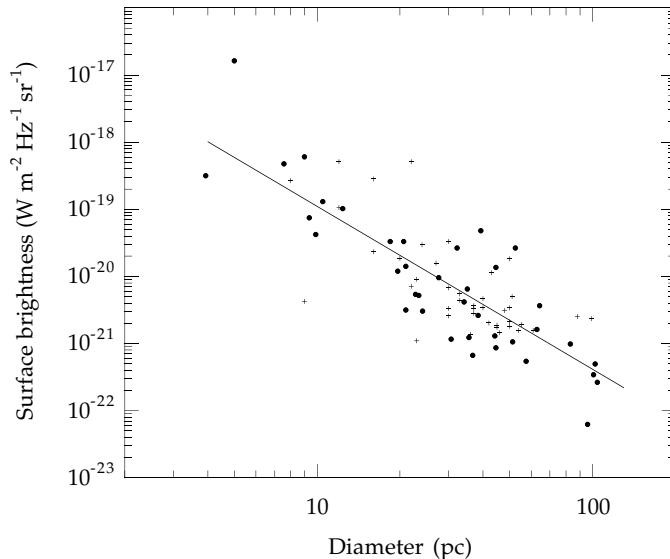


Fig. 4.— $\Sigma - D$ relation (Eq. 5) for the Galactic (solid dots) and LMC and SMC (crosses) shell SNRs. This fit includes 78 remnants and does not differ significantly from that with the Galactic SNRs alone (Eq. 3).

which sit far off the Galactic plane ($z \approx 600$ pc, $z \approx 250$ pc and $z \approx 300$ pc, respectively), and CTB 1. SNRs that are evolving at high z are likely expanding into regions of lower ambient density, which could effect their surface brightness evolution. If the seven SNRs with $z > 200$ pc (shown as open circles in Fig. 3) are excluded, the average fractional error is $\bar{f} = 0.33$.

An independent test of the accuracy of the $\Sigma - D$ relation was performed by using the extragalactic SNRs in the Large (LMC) and Small (SMC) Magellanic Clouds. Matthewson et al. (1983b) presented a catalog of 25 SNRs in the LMC (including 3 composites) and 6 in the SMC. They excluded the 4 Balmer-dominated remnants and derived a $\Sigma - D$ relation for the remaining 27 SNRs, obtaining a slope of $\beta = -2.6$. This slope is similar to that derived in Eq. 3, suggesting that the Galactic and extragalactic samples could be compared. Berkhuijsen (1986) gave an updated catalog of 41 shell SNRs in the LMC and SMC with known diameters and surface brightnesses. Eq. 3 was then applied to this sample and the fractional error calculated as above. The average fractional error for the LMC+SMC sample was $\bar{f} = 0.35$, less than that of the Galactic SNRs. All of the individual fractional errors for the LMC+SMC sample are less than $f = 0.8$ except for two (0505-679 and 0104-723), which had very large fractional errors ($f = 1.7$ and $f = 3.0$). If these two are excluded, the average fractional error is only $\bar{f} = 0.25$.

A $\Sigma - D$ relation can be derived for Berkhuijsen’s updated catalog. One SNR, 0505-679, lay far off the fit and was excluded in order to prevent it from unduly biasing the fit. The slope for the remaining 40 shell SNRs is $\beta = -2.44 \pm 0.34$, very near the slope in Eq. 3. The slope with all 41 shell SNRs is $\beta = -2.06 \pm 0.35$. The fact that i) the derived slopes of the $\Sigma - D$ relations for the two independent samples (Galactic and LMC+SMC) are consistent and ii) the application of the Galactic $\Sigma - D$ relation to the LMC+SMC sample yields an average fractional error of 0.25 gives us confidence in our derived Galactic $\Sigma - D$ relation. If the LMC and SMC SNRs are added to our sample of Galactic SNRs in Table 1, yielding

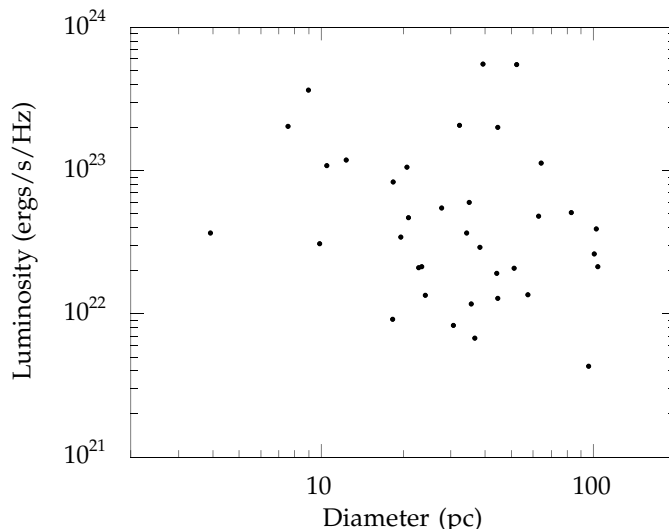


Fig. 5.— The radio luminosity (at 1 GHz) versus the diameter for the shell SNRs given in Table 1, excluding Cas A. No significant correlation is evident.

a total sample of 78 shell SNRs including Cas A and 0505-679, the combined fit for the $\Sigma - D$ relation is

$$\Sigma_{1\text{GHz}} = 2.82_{-1.43}^{+2.92} \times 10^{-17} D^{(-2.41 \pm 0.20)} \text{ W m}^{-2} \text{ Hz}^{-1} \text{ sr}^{-1} \quad (5)$$

and is shown in Figure 4. This is almost identical to the fit given in Eq. 3 but with smaller errors.

3. Discussion of $\Sigma - D$ Slope

The slope, β , of the $\Sigma - D$ relation derived here is much closer to $\beta = -2$ than for previous relations. The radio surface brightness is defined as

$$\Sigma_\nu \equiv 1.505 \times 10^{-19} \frac{S_\nu}{\theta^2} \text{ W m}^{-2} \text{ Hz}^{-1} \text{ sr}^{-1} \quad (6)$$

where S_ν is in Janskys and θ is in arcminutes. Using the definitions $D \propto \theta d$ (d being the distance to the remnant in kiloparsecs) and $L_\nu \propto S_\nu d^2$ (L_ν being the radio luminosity per unit frequency of the remnant), Eq. 6 becomes

$$\Sigma_\nu \propto L_\nu D^{-2}. \quad (7)$$

If L is independent of D , then β must be equal to -2 . The radio luminosities of the 36 SNRs in Table 1 (excluding Cas A) are plotted versus their diameters in Figure 5. Indeed, we do not find any significant correlation between luminosity and linear diameter for shell type alone or for shell plus composite type distance calibrators (see also Green 1991). However, the $\Sigma - D$ relation can be written as

$$\Sigma_\nu = AD^{-2+\delta} \quad (8)$$

to allow for a possible dependence of the luminosity on the linear diameter.

Duric & Seaquist (1986) derived a theoretical $\Sigma - D$ relation using the Sedov model for the evolution of the SNR blast wave and models for the magnetic field and particle acceleration in the remnant. They found that the magnitude of Σ depends on the initial supernova explosion energy, the ambient density and the strength and evolution of the magnetic field. Their diameter dependence of the surface brightness is

$$\Sigma \propto D^{-(\gamma+\gamma\alpha+3\alpha-1)} \quad (9)$$

where γ describes the magnetic field evolution and α is the radio spectral index. For reasonable values of γ used by Duric & Seaquist ($1.5 \leq \gamma \leq 2$) and typical values for α ($0.3 < \alpha < 0.8$), the slope of the $\Sigma - D$ relation lies in the range $-1.9 < \beta < -5$. All of the slopes derived thus far fall within this range. Σ could also depend on the evolutionary stage of the shell, in which case δ would be a function of the age of the SNR, or on any interactions of the shell with nearby objects (such as molecular clouds or H II regions). Any $\Sigma - D$ type relation must explicitly take the factors discussed above into account before more accurate distances can be estimated for *individual* SNRs.

Several studies have been done to try and improve the $\Sigma - D$ fit. Caswell & Lerche (1979) and Milne (1979) investigated the dependence of the radio surface brightness on the Galactic height, z , using separate methods. However, these studies rely upon only a few high z remnants and therefore the results are not well constrained. As noted earlier, when the SNRs with $z > 200$ pc were excluded, the average fractional error decreased, possibly indicating a different surface brightness evolution for these high z remnants. But when we examined the z -dependence of the surface brightness for the remnants in Table 1, no clear correlation was found (see also Green 1984, Allakhverdiyev et al. 1983b). This does not preclude a z -dependence, but more high z remnants are needed to adequately address this question.

Huang & Thaddeus (1985) suggested using a subsample of SNRs that are evolving into similar environments to reduce the scatter in the $\Sigma - D$ relation. They used 12 SNRs (including Cas A and W44, which we consider a composite) situated near molecular cloud complexes and determined distances to the remnants by using the optical distances to H II regions or OB associations associated with the cloud or from CO emission from the cloud itself. The $\Sigma - D$ relation they derive has a slope of -3.21 ± 0.32 with less scatter than previous relations. More up-to-date distances (kinematic distances recalculated using a modern rotation curve or more reliable distance estimates) are available for some of the SNRs, and we find that the slope flattens to $\beta = -3.02 \pm 0.44$ for the same 12 remnants when the new distances are used (although the slopes are consistent within errors). Huang and Thaddeus excluded one remnant (HB 9) simply because it lay too far off their $\Sigma - D$ fit. If we use a more recent distance estimate to HB 9 (see Table 2) and then include it in the fit, we obtain $\beta = -2.88 \pm 0.40$ for the 13 SNRs. Excluding the composite remnant W44, leaving 12 shell SNRs, does not significantly change the fit parameters. This value for the slope agrees, within the errors, to the value derived in Eq. 2. Notice that using more up-to-date distances has the effect of flattening the slope of the $\Sigma - D$ relation.

Also, we have shown that adding the shell SNRs in the LMC and SMC to the Galactic sample decreases the errors in the fit for the $\Sigma - D$ relation.

As Eqs. 7, 8 and 9 suggest, the $\Sigma - D$ relation is *only* valid for use in estimating distances to individual SNRs when the following assumptions are made, namely that all shell SNR radio luminosities have the same diameter dependence and that all shell SNRs are born under the same initial conditions (same supernova explosion energy, density and structure of environment, magnetic field, etc.). For the SNRs with known distances, there can be almost 2 orders of magnitude variation in luminosity for a given diameter (see Fig. 5). It should be understood then that this variation in individual SNR luminosities gives rise to the uncertainty in the distance estimates derived from the $\Sigma - D$ relation. However, while on average the errors

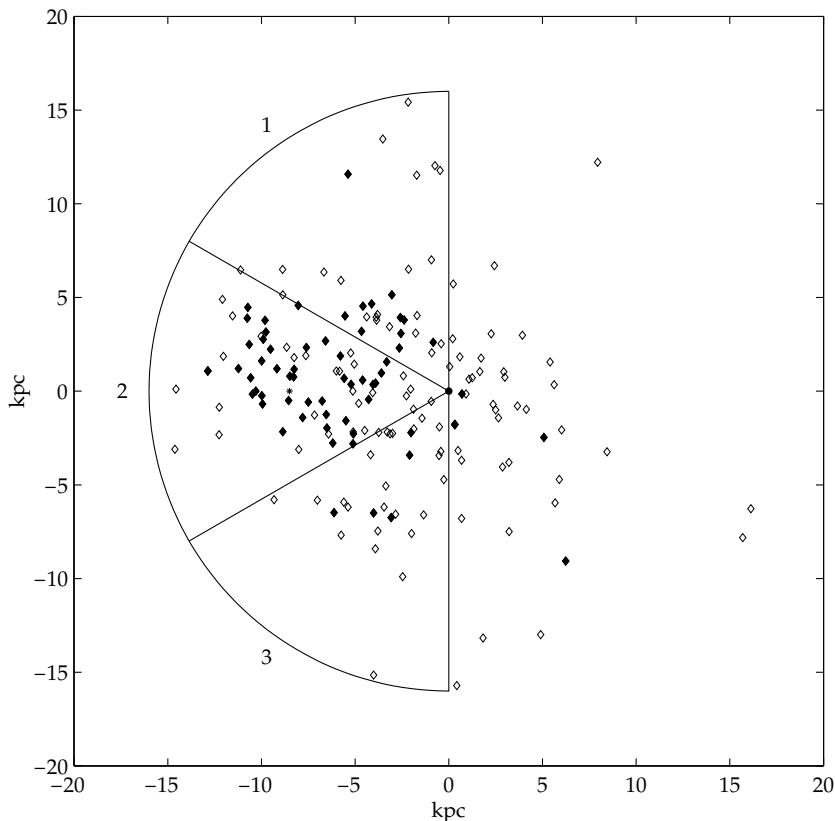


Fig. 6.— The Galactic SNR distribution using corrected distances and our new $\Sigma - D$ relation. Filled-center and composite SNRs with known distances are included. Shell SNRs with distances derived from our $\Sigma - D$ relation (c.f. Table 3) are shown as open diamonds, while SNRs with known distances are shown as filled diamonds. The filled circle marks the Galactic Center and the ‘*’ marks the position of the Sun. Also shown are the three regions into which the near half of the Galaxy is divided. (see §4).

in the individual distances are $\approx 40\%$, the errors in ensemble studies of SNRs utilizing the $\Sigma - D$ relation can be much smaller (as will be shown). If the aforementioned assumptions are made, keeping in mind the implied limitations, $\Sigma - D$ distances can be used to estimate ensemble properties such as the SNR surface density distribution and the total number of SNRs in the Galaxy. Using the the $\Sigma - D$ relation in Eq. 3, the distances were calculated to all shell SNRs for which no other distance information is available. These remnants and their distances are listed in Table 3. For reasons stated above, caution should be exercised in using the distances to individual SNRs in given Table 3. Figure 6 shows the positions of all remnants of all types with known (including recalculated) distances (plotted as filled diamonds) as well as shell SNRs with distances obtained from the new $\Sigma - D$ relation (plotted as open diamonds). In total 178 remnants are shown.

Table 3. Distances to shell SNRs calculated from $\Sigma - D$ relation

Name	$\Sigma_{1\text{GHz}}^{\text{a}}$ ($\text{W m}^{-2} \text{ Hz}^{-1} \text{ s}^{-1}$)	θ^{b} ($'$)	d (kpc)
G0.0+0.0.	1.7×10^{-18}	3.5×2.5	3.3
G1.0-0.1..	4.6×10^{-20}	8	5.6
G1.4-0.1..	3.0×10^{-21}	10	14.1
G1.9+0.3.	6.3×10^{-20}	1.2	32.8
G3.7-0.2..	2.9×10^{-21}	11×14	11.5
G3.8+0.3.	1.9×10^{-21}	18	9.6
G4.2-3.5..	6.1×10^{-22}	28	9.8
G5.2-2.6..	1.2×10^{-21}	18	11.5
G5.9+3.1.	1.2×10^{-21}	20	10.2
G6.4+4.0.	2.0×10^{-22}	31	14.1
G7.7-3.7..	3.4×10^{-21}	22	6.1
G8.7-5.0..	9.8×10^{-22}	26	8.7
G9.8+0.6.	4.1×10^{-21}	12	10.4
G11.4-0.1.	1.4×10^{-20}	8	9.2
G13.5+0.2	2.6×10^{-20}	5×4	12.7
G15.1-1.6.	1.1×10^{-21}	30×24	7.9
G15.9+0.2	1.9×10^{-20}	7×5	11.1
G17.4-2.3.	1.3×10^{-21}	24	8.5
G17.8-2.6.	1.0×10^{-21}	24	9.2
G21.8-0.6.	2.6×10^{-20}	20	2.9
G22.7-0.2.	7.3×10^{-21}	26	3.7
G23.3-0.3.	1.4×10^{-20}	27	2.7
G24.7-0.6.	5.4×10^{-21}	15	7.4
G28.8+1.5	^c	100	^c
G30.7+1.0	2.1×10^{-21}	24×18	7.9
G31.5-0.6.	9.3×10^{-22}	18	12.9
G32.0-4.9.	9.2×10^{-22}	60	3.9
G32.8-0.1.	5.7×10^{-21}	17	6.3
G33.2-0.6.	1.6×10^{-21}	18	10.2
G36.6-0.7.	^c	25	^c
G36.6+2.6	4.8×10^{-22}	17×13	20.6
G39.2-0.3.	5.6×10^{-20}	8×6	5.9
G40.5-0.5.	3.4×10^{-21}	22	6.1
G41.1-0.3.	2.9×10^{-19}	4.5×2.5	6.1
G42.8+0.6	7.8×10^{-22}	24	10.4
G43.9+1.6	3.6×10^{-22}	60	5.7
G45.7-0.4.	1.3×10^{-21}	22	9.1
G55.7+3.4	4.0×10^{-22}	23	14.4
G57.2+0.8	1.9×10^{-21}	12	14.3

Table 3—Continued

Name	$\Sigma_{1\text{GHz}}^{\text{a}}$ ($\text{W m}^{-2} \text{ Hz}^{-1} \text{ s}^{-1}$)	θ^{b} ($'$)	d (kpc)
G59.5+0.1.	1.8×10^{-20}	5	13.3
G65.1+0.6.	2.0×10^{-22}	90×50	6.6
G65.3+5.7.	1.1×10^{-22}	310×240	2.1
G67.7+1.8.	2.6×10^{-21}	9	16.7
G69.7+1.0.	9.4×10^{-22}	16	14.4
G73.9+0.9.	2.8×10^{-21}	22	6.6
G82.2+5.3.	2.9×10^{-21}	95×65	1.8
G84.9+0.5.	3.3×10^{-21}	6	22.5
G93.3+6.9.	2.5×10^{-21}	27×20	6.6
G93.7-0.2..	1.5×10^{-21}	80	2.3
G94.0+1.0.	3.0×10^{-21}	30×25	5.2
G112.0+1.2	1.2×10^{-21}	30	7.0
G117.4+5.0	9.4×10^{-22}	60×80	3.3
G126.2+1.6	2.1×10^{-22}	70	6.1
G127.1+0.5	9.7×10^{-22}	45	5.1
G152.2-1.2.	2.0×10^{-22}	110	6.6
G179.0+2.6	2.1×10^{-22}	70	6.1
G192.8-1.1.	4.9×10^{-22}	78	3.9
G206.9+2.3	3.8×10^{-22}	60×40	6.9
G211.7-1.1.	4.6×10^{-22}	70	4.4
G261.9+5.5	1.3×10^{-21}	40×30	5.9
G272.2-3.2.	^c	15	^c
G279.0+1.1	5.0×10^{-22}	95	3.2
G284.3-1.8.	2.9×10^{-21}	24	6.0
G286.5-1.2.	1.4×10^{-21}	26×6	15.1
G289.7-0.3.	3.7×10^{-21}	18×14	8.2
G294.1-0.0.	^c	40	^c
G296.1-0.5.	1.3×10^{-21}	37×25	6.6
G296.8-0.3.	4.8×10^{-21}	20×14	6.9
G298.6-0.0.	7.0×10^{-21}	12×9	9.5
G299.2-2.9.	3.8×10^{-22}	18×11	23.9
G299.6-0.5.	8.9×10^{-22}	13	18.1
G301.4-1.0.	3.7×10^{-22}	37×23	11.7
G302.3+0.7	2.6×10^{-21}	17	8.8
G308.1-0.7.	1.1×10^{-21}	13	16.8
G309.2-0.6.	5.9×10^{-21}	15×12	8.0
G310.6-0.3.	1.2×10^{-20}	8	10.0
G310.8-0.4.	6.3×10^{-21}	12	8.6
G312.4-0.4.	4.7×10^{-21}	38	3.1

Table 3—Continued

Name	$\Sigma_{1\text{GHz}}^{\text{a}}$ ($\text{W m}^{-2} \text{ Hz}^{-1} \text{ s}^{-1}$)	θ^{b} ($'$)	d (kpc)
G315.4-0.3.	3.9×10^{-21}	24×13	7.2
G315.9-0.0.	3.4×10^{-22}	25×14	18.8
G316.3+0.0	7.4×10^{-20}	29×14	1.8
G317.3-0.2.	5.8×10^{-21}	11	9.7
G318.2+0.1	c	40×35	c
G320.6-1.6.	c	60×30	c
G321.9-1.1.	c	28	c
G321.9-0.3.	2.7×10^{-21}	31	5.5
G323.5+0.1	2.7×10^{-21}	15	11.4
G327.4+0.4	1.0×10^{-20}	21	4.0
G327.4+1.0	1.8×10^{-21}	14	13.9
G329.7+0.4	c	40×33	c
G330.2+1.0	6.2×10^{-21}	11	9.5
G332.4+0.1	1.7×10^{-20}	15	4.5
G335.2+0.1	5.5×10^{-21}	21	5.2
G336.7+0.5	6.5×10^{-21}	14×10	8.7
G337.0-0.1.	2.8×10^{-20}	13×7	5.8
G337.2-0.7.	8.4×10^{-21}	6	15.3
G337.3+1.0	1.3×10^{-20}	15×12	5.6
G337.8-0.1.	5.0×10^{-20}	9×6	5.9
G338.1+0.4	2.7×10^{-21}	15	9.9
G338.3+0.0	1.6×10^{-20}	8	8.6
G340.4+0.4	9.4×10^{-21}	10×7	10.5
G340.6+0.3	3.3×10^{-20}	6	8.6
G341.9-0.3.	7.2×10^{-21}	7	14.0
G342.0-0.2.	4.9×10^{-21}	12×9	11.1
G342.1+0.9	8.4×10^{-22}	10×9	25.5
G343.1-0.7.	2.1×10^{-21}	27×21	6.9
G345.7-0.2.	2.5×10^{-21}	6	25.4
G346.6-0.2.	1.9×10^{-20}	8	8.2
G348.5-0.0.	1.5×10^{-20}	10	7.2
G349.2-0.1.	3.9×10^{-21}	9×6	17.2
G350.0-1.8.	5.2×10^{-21}	30	3.7
G351.7+0.8	6.0×10^{-21}	18×14	6.7
G351.9-0.9.	2.5×10^{-21}	12×9	14.7
G352.7-0.1.	1.3×10^{-20}	8×6	11.2
G354.8-0.8.	1.2×10^{-21}	19	11.1
G355.6+0.0	9.4×10^{-21}	6×8	12.6

Table 3—Continued

Name	$\Sigma_{1\text{GHz}}^{\text{a}}$ ($\text{W m}^{-2} \text{ Hz}^{-1} \text{ s}^{-1}$)	θ^{b} ($'$)	d (kpc)
G355.9-2.5.	7.1×10^{-21}	13	7.6
G356.3-1.5.	1.5×10^{-21}	15×20	10.9
G356.3-0.3.	5.9×10^{-21}	7×11	12.2
G357.7+0.3	2.6×10^{-21}	24	6.2
G359.0-0.9.	6.5×10^{-21}	23	4.4
G359.1+0.9	5.7×10^{-21}	11×12	9.4

^aSurface brightnesses are calculated from fluxes and angular diameters given in Green’s SNR Catalog (1996a) and Eq. 6 in text.

^bFor roughly circular SNRs, a single diameter is given, while for elliptical SNRs, the angular sizes of the major and minor axes of the ellipse are given. Angular diameters are taken from Green’s SNR Catalog (1996a).

^cNo 1 GHz surface brightness is available because radio observations of these SNRs have not been made at enough frequencies, preventing an extrapolation of the measured surface brightnesses to 1 GHz. Consequently, no distance was derived for these remnants.

4. Selection Effects and the SNR Distribution

It is of interest to determine the radial distribution of the Galactic shell SNRs. In order to obtain a truer picture of the distribution, the problem of selection effects inherent in SNR searches must be addressed. Previously, Ilovaisky & Lequeux (1972) used a derived luminosity distribution to correct for selection effects, and based on that, suggested a flat SNR distribution out to 8 kpc and a sharp cutoff beyond 10 kpc. Kodaira (1974) used empirically determined scaling factors for selection effects and obtained a radial distribution peaked at smaller Galactic radii (~ 5 kpc). Van den Bergh (1988b) suggested that the fact that the longitudinal distribution of SNRs showed a high, uniform concentration between $55^\circ < l < 345^\circ$ could indicate that most of the SNRs in that region reside in a nuclear ring with $R = 6.5$ kpc. Leahy & Xinji (1989) assumed circular symmetry around the Galactic Center and near completeness of the observations within 2 kpc of the Sun. Using a series of successive corrections, they derived an SNR surface density distribution similar to Kodaira’s and estimated the total number of SNRs in the Galaxy with $\Sigma > 3 \times 10^{-22} \text{ W m}^{-2} \text{ Hz}^{-1} \text{ sr}^{-1}$ to be $(485 \pm 60)/f_1$, where f_1 is the completeness factor within 2 kpc.

To compensate for observational selection effects we follow a method devised by Narayan (1987) for pulsar distributions. This involves calculating a scale factor which is the ratio of the number of the predicted shell SNRs in a specified volume to the number of observable shell SNRs in that volume. This scale factor is determined as a function of Galactic position,

$$S(r, \phi) = \frac{\int f(\Sigma) d\Sigma}{\int_{obs} f(\Sigma) d\Sigma}, \quad (10)$$

where $f(\Sigma)$ is the functional form of the distribution of shell SNR surface brightnesses and r and ϕ are the Galactic radius and azimuth. In order to calculate the scale factors, it is necessary to ascertain the true SNR surface brightness distribution. Following Li et al. (1991), we assume that the observational surveys for shell SNRs are sufficiently complete within 3 kpc of the Sun (this is justified by the scale factors that are calculated for that region—see below), and that distribution is taken to be representative of $f(\Sigma)$ in the entire Galaxy. The resulting Σ distribution is shown in Figure 2 and can be approximated as a Gaussian with a lower cutoff at $\Sigma_c = 5 \times 10^{-23} \text{ W m}^{-2} \text{ Hz}^{-1} \text{ sr}^{-1}$, corresponding to a remnant age $t \approx 10^6$ years.

The Galaxy is divided into bins of $1 \text{ kpc} \times 10^\circ$ in r and ϕ . A random r and ϕ are chosen inside a bin (all points are chosen at $z = 0$), and for this point, a corresponding random point is chosen on $f(\Sigma)$. One is added to the numerator. Next, based upon its surface brightness and angular size, it is determined whether this SNR would be seen by the any of the selected radio telescope surveys that were conducted in that sky bin. Based on their sensitivities, observing frequencies and amount of sky coverage, five telescopes were chosen: Effelsberg 100-m, Parkes 64-m, Dominion Royal Astronomy Observatory, Westerbork Synthesis Radio Telescope and Molonglo Observatory Synthesis Telescope. The surveys are listed in Table 4. For the single dish telescopes (Effelsberg and Parkes) the survey sensitivities were calculated following Christiansen & Högbom (1985)

$$S_{min} = \frac{2QMk(T_{rec} + T_{sky})}{\sqrt{(\Delta\nu t)A_{eff}}}, \quad (11)$$

where Q is the minimum detection significance (here taken to be 5), M is a numerical factor dependent upon the type of telescope, k is the Boltzman constant, T_{rec} is the receiver noise temperature, T_{sky} is the background sky temperature, $\Delta\nu$ is the bandwidth, t is the integration time, and $A_{eff} = \eta_a \eta_b A_{geo}$ is the effective area of the telescope, with η_a and η_b being the antenna and beam efficiencies, respectively. The telescope parameters were taken from the references given in Table 4. The sky temperature, as a function of Galactic longitude and latitude, was measured by Haslam et al. (1982) at 408 MHz. Their results were

fit by Narayan (1987) to give

$$T_{sky,408}(l, b) = 25 + \frac{275}{\left(1 + (l/42)^2\right) \left(1 + (b/3)^2\right)} \text{ K.} \quad (12)$$

This temperature can be generalized to other frequencies using the frequency dependence derived by Lawson et al. (1987)

$$T_{sky}(\nu) = T_{sky,408} \left(\frac{408}{\nu}\right)^{2.6} \text{ K.} \quad (13)$$

For the synthesis telescopes, the sensitivity limit is taken as 5 times the rms noise in the maps (see Table 4 for references). If the SNR could be detected by at least one of the telescopes surveys that have observed that sky bin, 1 is added to the denominator. By repeating for a large number of positions on $f(\Sigma)$ an approximate value for $S(r, \phi)$ is obtained for each bin.

This scale factor is then multiplied by the number of SNRs actually observed to give the corrected number of SNRs in that bin. For bins inside the Solar Circle where there are no observed SNRs (hereafter referred to as zero bins), two different methods were evaluated (and ultimately not used) to assign a corrected value to these bins. First, for zero bins which had nonzero bins on either side (in the azimuthal direction), the two neighboring bins were averaged and that value assigned to the zero bin. The second method, used when two or more consecutive bins had no observed SNRs, utilizes Poisson statistics. There is a 50% Poisson probability of observing zero if the expected number is 0.7. This number (0.7) was divided evenly among the zero bins. However, if this method was applied to the case of an isolated zero bin, only 0.7 would be added, whereas a minimum of 1 would have been added using the first method. It was eventually decided that neither method would be employed, as the two methods did not agree for isolated zero bins, and consecutive zero bins may not be expected to have any SNRs observed in them (e. g. inter-arm regions of the Galaxy). Therefore, no compensation is made for a bin where there are no SNRs observed; the corrected number is still zero in that bin.

The errors in the scale factors are typically $\sim 10\%$, due mainly to the uncertainty in the lower cut-off employed in the surface brightness distribution, $f(\Sigma)$, and the telescope sensitivities. A completeness factor, f_c , which is essentially the inverse of the area-weighted average scale factor, can be estimated to reflect the level of observational completeness. The completeness factor is fairly constant at $f_c \approx 0.98$ until $r = 2.5 - 3$ kpc, after which the completeness factor begins to drop off, justifying our assumption of observational completeness out to 3 kpc (see Fig. 2). Completeness factors, f_z , which are the inverse of the area-weighted average scale factors only for the zero bins, can also be estimated to reflect the level incompleteness due to zero bins. For the entire near half of the Galaxy (see Fig. 6), $f_z \sim 0.85$ for $\Sigma > 5 \times 10^{-23} \text{ W m}^{-2} \text{ Hz}^{-1} \text{ sr}^{-1}$. For the region within 3 kpc of the Sun, $f_z \approx 0.99$.

The bins, corrected for selection effects, are combined into three broad regions in azimuth. These regions are shown in Fig. 6. The apparent absence of SNRs in the outer portion of region 3 is probably real, due to the outer spiral arms ending before reaching this region. The bins in each region are combined further in azimuth to obtain a single radial profile for that region and converted to surface densities. When 1 kpc radial bins were used, peaks in the radial distribution show a rough correspondence to the positions of the spiral arms. In order to get an estimate of the errors in the shell SNR surface densities due to the uncertainty in the $\Sigma - D$ relation, a Monte Carlo simulation was used, taking the fractional errors of Fig 3 into account, in order to obtain bootstrapped errors. The errors in the densities are typically $\sim 10 - 20\%$ in the mid-regions of the Galaxy ($r \approx 4 - 12$ kpc) and considerably higher (up to 75%) in the regions of low statistics ($r \leq 4$ kpc, $r \geq 12$ kpc). The scale factors cannot compensate for bins where no SNRs

Table 4. Telescope surveys used in calculating scale factors

Telescope	Survey area (deg)		Angular res. (arcmin)	Freq. (GHz)	Ref.
	long.	lat.			
Effelsberg 100-m	$357 \leq l \leq 76$	$ b \leq 1.5$	4.3	2.7	1
	$76 \leq l \leq 240$	$ b \leq 5$	4.3	2.7	2
	$357 \leq l \leq 95$	$ b \leq 4$	9.4	1.41	3
Parkes 64-m	$206 \leq l \leq 49$	$-2 \leq b \leq 3.5$	4.0	5.0	4
	$288 \leq l \leq 307$	$ b \leq 2$	8.2	2.7	5
	$307 \leq l \leq 330$	$ b \leq 2$	8.2	2.7	6
	$334 \leq l \leq 345$	$ b \leq 2$	8.2	2.7	7
	$345 \leq l \leq 5$	$ b \leq 2$	7.4	2.7	8
	$6 \leq l \leq 26$	$ b \leq 2$	8.2	2.7	9
	$37 \leq l \leq 47$	$ b \leq 2$	8.2	2.7	10
Dominion Royal Astronomy Observatory	$81 \leq l \leq 89$	$-2.5 \leq b \leq 5.5$	4.8×3.5	.408	11
	$81 \leq l \leq 89$	$-2.5 \leq b \leq 5.5$	1.4×1.0	1.42	11
	$101 \leq l \leq 109$	$-2 \leq b \leq 6$	3.9×3.4	.408	12
	$101 \leq l \leq 109$	$-2 \leq b \leq 6$	1.2×1.0	1.42	12
	$136 \leq l \leq 144$	$-2 \leq b \leq 6$	3.8×3.4	.408	13
	$136 \leq l \leq 144$	$ b \leq 4$	1.1×1.0	1.42	13
Westerbork Synthesis Radio Telescope	$44 \leq l \leq 90$	$ b \leq 1.5$	$1 \times 1 \text{ csc } \delta$.327	14
Molonglo Observatory Synthesis Telescope . . .	$335 \leq l \leq 5$	$ b \leq 2.5$	$.73 \times .73 \text{ csc } \delta$.843	15
	$240 \leq l \leq 355$	$ b \leq 1.5$	$.73 \times .73 \text{ csc } \delta$.843	16

References. — (1) Reich et al. 1984; (2) Fürst et al. 1990; (3) Reich, Reich & Fürst 1990; (4) Shaver & Goss 1970; (5) Thomas & Day 1969a; (6) Day, Thomas & Goss 1969; (7) Thomas & Day 1969b; (8) Beard, Thomas & Day 1969; (9) Goss & Day 1969; (10) Day, Warne & Cooke 1969; (11) Normandeau, Joncas & Green 1992; (12) Joncas & Higgs 1990; (13) Green 1989a; (14) Taylor, Wallace & Goss 1992; (15) Gray 1994; (16) Whiteoak & Green 1996

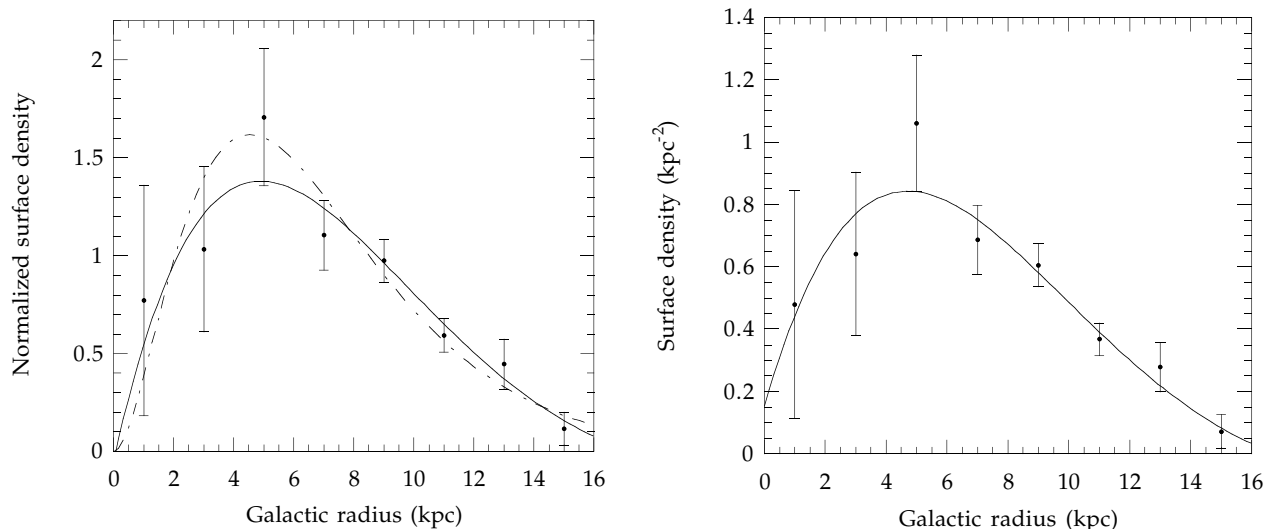


Fig. 7.— The SNR density radial distribution for Region 2 using the new distances and compensation for selection effects. (a) The distribution derived in this work (solid line and data points) and that of Kodaira (1974) (dashed line), both normalized to the density at the radius of the Solar Circle. (b) The unnormalized data points and the fit to Eq. 15.

are observed, and therefore observational incompleteness is still a problem for regions 1 and 3, where the completeness factors are lower. The scaled total number of shell SNRs in region 2 is $(56 \pm 4)/f_z$, where the error on the number of SNRs represents the uncertainty in the $\Sigma - D$ relation and f_z represents the incompleteness due to the lack of selection effects compensation for the zero bins. For region 2, $f_z \approx 0.96$. If region 2 is considered representative of the entire Galaxy, then the total number of shell remnants for $r \leq 16$ kpc and $\Sigma > 5 \times 10^{-23}$ W m⁻² Hz⁻¹ sr⁻¹ is estimated to be $336/f_z$. The Monte Carlo simulation shows that this estimate is not very sensitive to the uncertainty in the $\Sigma - D$ relation.

A weighted fit of the shell SNR surface density distribution in region 2, normalized to the surface density at the Solar Circle, was performed using the functional form employed by Stecker & Jones (1977),

$$f(r) = \left(\frac{r}{r_\odot}\right)^\alpha \exp\left(-\beta \frac{r - r_\odot}{r_\odot}\right), \quad (14)$$

where $r_\odot = 8.5$ kpc is the Sun-Galactic Center distance. We find that $\alpha = 2.00 \pm 0.67$ and $\beta = 3.53 \pm 0.77$; the radial scale length of the distribution is ≈ 7.0 kpc. The shape of the distribution is similar to that obtained by Kodaira (1974). The two distributions are shown in Figure 7a.

Equation 14 implies that the surface density is zero at $r = 0$. However, our data suggest that the surface density is not zero near the Galactic Center. Therefore, we have used the following functional form to obtain a weighted fit to the unnormalized surface density distribution:

$$f(r) = A \sin\left(\frac{\pi r}{r_0} + \theta_0\right) e^{-\beta r} \quad (15)$$

where $A = 1.96 \pm 1.38 \text{ kpc}^{-2}$, $r_0 = 17.2 \pm 1.9 \text{ kpc}$, $\theta_0 = 0.08 \pm 0.33$ and $\beta = 0.13 \pm 0.08 \text{ kpc}^{-1}$. This fit is valid for $r < r_o(1 - \theta_o/\pi)$, i.e. 16.8 kpc; $f(r) = 0$ beyond that. The data and fit are shown in Figure 7b.

The scale length of 7.0 kpc is consistent with that determined by previous studies. Green (1996b) used a simple model with SNRs distributed as a gaussian in Galactic radius and compared the resulting longitudinal distribution to the observed SNR longitudinal distribution, obtaining a scale length of ≈ 7.0 kpc. However, no attempt was made to compensate for selection effects other than to use a Σ -limited sample. Li et al. (1991) used a more sophisticated model distributing SNRs in an exponential disk as well as in spiral arms. They incorporated a $1/d^2$ selection bias, assuming completeness out to $d = 3$ kpc. They then compared the longitudinal distribution given by the model with the observed SNR longitudinal distribution, obtaining a scale length of $\approx 5 - 9$ kpc, depending on the model parameters. As Li et al. point out, the scale length of the Galactic stellar disk is ~ 5 kpc, suggesting that the SNR scale length, as derived in this work and by Green (1996b) and Li et al. (1991), would indicate that the SNR distribution is not associated with the stellar disk population.

5. Conclusion

The catalogue of known SNRs has continued to grow in size. The number of SNRs with reasonably determined distances has also increased. However, most distances given in the literature were calculated using older rotation curves. We have recalculated the distances, where necessary, using a modern rotation curve, and used the updated distances to derive a new $\Sigma - D$ relation for shell SNRs. This $\Sigma - D$ relation, using a sample of 36 shell SNRs (37 including Cas A), yields a slope of -2.38 excluding Cas A and -2.64 with Cas A. When the 41 shell SNRs in the LMC and SMC are added to the sample, the slope is -2.41 with a smaller error. Using the $\Sigma - D$ relation to estimate distances to individual remnants is viable only with the assumptions that all shell SNRs have the same radio luminosity dependence on linear diameter, the same supernova explosion mechanism and energy, and are evolving into identical environments. We find that, on average, the error in the distance estimation to an individual SNR to be $\sim 40\%$ when using our $\Sigma - D$ relation. However, the error in deriving ensemble characteristics of SNRs such as the SNR surface density can be lower ($\sim 10 - 20\%$ for the mid-galactic region). We attempt to compensate for observational selection effects inherent in SNR searches by employing a scaling method based on the sensitivity, angular resolution, and sky coverage of actual radio surveys. Utilizing the updated distances, the new $\Sigma - D$ relation and the scale factors, the shell SNR surface density radial distribution was derived. The distribution peaks at ~ 5 kpc and has a scale length of ~ 7.0 kpc.

We would like to thank Robert Hurt for useful discussion on radio telescope surveys, as well as anonymous referees for helpful suggestions. We also would like to thank the staff of the U. C. Riverside IGPP for their support. This work was supported in part by NASA through the grant NAGW-1996.

REFERENCES

- Allakhverdiyev, A. O., Amnuel, P. R., Gueinov, O. H., & Kasumov, F. K. 1983a, *Ap&SS*, 97, 261
———, 1983b, *Ap&SS*, 97, 287
- Anderson, S. B., Cadwell, B. J., Jacoby, B. A., Wolszczan, A., Foster, R. S., & Kramer, M. 1996, *ApJ*, 468, L55
- Bandiera, R. 1987, *ApJ*, 319, 885
- Beard, M., Thomas, B. MacA., & Day, G. A. 1969, *Aust. J. Phys.*, 11, 27
- Berkhuijsen, E. M. 1986, *A&A*, 166, 257
- Burton, W. B., & Gordon, M. A. 1978, *A&A*, 63, 7
- Caswell, J. L., & Lerche, I. 1979, *MNRAS*, 187, 201
- Caswell, J. L., Murray, J. D., Roger, R. S., Cole, D. J., & Cooke, D. J. 1975, *A&A*, 45, 239
- Christiansen, W. N., & Högbom, J. A. 1985, *Radiotelescopes*, 2nd ed. (New York: Cambridge Univ. Press)
- Clark, D. H., & Caswell, J. L. 1976, *MNRAS*, 174, 267
- Clemens, D. P. 1985, *ApJ*, 295, 422
- Davelaar, J., Smith, A., & Becker, R. H. 1993, *ApJ*, 300, L59
- Day, G. A., Thomas, B. MacA., & Goss, W. M. 1969, *Aust. J. Phys.*, 11, 11
- Day, G. A., Warne, W. G., & Cooke, D. J. 1969, *Aust. J. Phys.*, 13, 11
- Dubner, G. M., Colomb, F. R., & Gianciani, E. B. 1986, *AJ*, 91, 343
- Duric, N., & Seaquist, E. R. 1986, *ApJ*, 301, 308
- Feldt, C., & Green, D. A. 1993, *A&A*, 274, 421
- Fesen, R. A. 1984, *ApJ*, 281, 658
- Fesen, R. A., Becker, R. H., & Blair, W. P. 1987, *ApJ*, 313, 378
- Fich, M., Blitz, L., & Stark, A. A. 1989, *ApJ*, 342, 272
- Frail, D. A., & Clifton, T. R. 1989, *ApJ*, 336, 854
- Frail, D. A., Goss, W. M., & Whiteoak, J. B. Z. 1994, *ApJ*, 437, 781
- Fürst, E., Reich, W., Reich, P., & Reif, K. 1990, *A&AS*, 85, 691
- Goss, W. M., & Day, G. A. 1969, *Aust. J. Phys.*, 13, 3
- Gray, A. D. 1994, *MNRAS*, 270, 822
- Green, D. A. 1984, *MNRAS*, 209, 449

- 1989a, *A&AS*, 78, 277
- 1989b, *MNRAS*, 238, 737
- 1991, *PASP*, 103, 209
- 1996a, A Catalog of Galactic Supernova Remnants (August 1996 version), Mullard Radio Astronomy Observatory, Cambridge, United Kingdom (available on the World Wide Web at “<http://www.phy.cam.ac.uk/www/research/ra/SNRs/snrs.intro.html>”)
- 1996b, in *IAU Colloquium 145, Supernovae and Supernova Remnants*, ed. R. McCray & Z. Wang (Cambridge: Cambridge Univ. Press), 341
- Hailey, C. J., & Craig, W. W. 1994, *ApJ*, 434, 635
- Haslam, C. G. T., Salter, C. J., Stoffel, H., & Wilson, W. E. 1982, *A&AS*, 47, 1
- Huang, Y.-L., & Thaddeus, P. 1985, *ApJ*, 295, L13
- Ilovaisky, S. A., & Lequeux, J. 1972, *A&A*, 18, 169
- Joncas, G., & Higgs, L. A. 1990, *A&AS*, 82, 113
- Junkes, N., Fürst, E., & Reich, W. 1992, *A&AS*, 96, 1
- Kamper, K., & van den Bergh, S. 1976, *ApJS*, 32, 351
- Kassim, N. E., Hertz, P., Van Dyk, S. D., & Weiler, K. W. 1994 *ApJ*, 427, L95
- Kodaira, K. 1974, *PASJ*, 26, 255
- Koo, B.-C., Kim, K.-T., & Seward, F. D. 1995, *ApJ*, 447, 211
- Landecker, T. L., Pineault, S., Routledge, D., & Vaneldik, J. F. 1989, *MNRAS*, 237, 277
- Lawson, K. D., Mayer, C. J., Osborne, J. L., & Parkinson, M. L. 1987, *MNRAS*, 225, 307
- Leahy, D. A., Nousek, J., & Hamilton, A. J. S. 1991, *ApJ*, 374, 218
- Leahy, D. A., & Xinji, W. 1989, *PASP*, 101, 607
- Li, Z. W., & Wheeler, J. C. 1984, *BAAS*, 16, 334
- Li, Z. W., Wheeler, J. C., Bash, F. N., & Jefferys, W. H. 1991, *ApJ*, 378, 93
- Long, K. S., Blair, W. P., & van den Bergh, S. 1988, *ApJ*, 333, 749
- Lozinskaya, T. A. 1981, *SvAL*, 7, 17
- Matthewson, D. S., Ford, V. L., Dopita, M. A., Tuohy, I. R., Long, K. S., & Helfand, D. J. 1983a, in *IAU Symposium 101, Supernova Remnants and Their X-ray Emission*, ed. J. Danziger & P. Gorenstein (Dordrecht: Reidel), 541
- Matthewson, D. S., Ford, V. L., Dopita, M. A., Tuohy, I. R., Long, K. S., & Helfand, D. J. 1983b, *ApJS*, 51, 345

- Milne, D. K. 1979, *Aust. J. Phys.*, 32, 83
- Minkowski, D. 1958, *Rev. Mod. Phys.*, 30, 1048
- Narayan, R. 1987, *ApJ*, 319, 162
- Normandeau, M., Joncas, G., & Green, D. A. 1992, *A&AS*, 92, 63
- Normandeau, M., Taylor, A. R., & Dewdney, P. E. 1997, *ApJS*, 108, 279
- Odegard, N. 1986, *ApJ*, 301, 813
- Pfeffermann, E., Aschenbach, B., & Predehl, P. 1991, *A&A*, 246, L28
- Pineault, S., Landecker, T. L., Madore, B., & Gaumont-Guay, S. 1993, *AJ*, 105, 1060
- Radhakrishnan, V., Goss, W. M., Murray, J. D., & Brooks, J. W. 1972, *ApJS*, 24, 49
- Reed, J. E., Hester, J. J., Fabian, A. C., & Winkler, P. F. 1995, *ApJ*, 440, 706
- Reich, W., & Braunsfurth, E. 1981, *A&A*, 99, 17
- Reich, W., Fürst, E., & Arnal, E. M. 1992, *A&A*, 256, 214
- Reich, W., Fürst, E., Steffen, P., Reif, K., & Haslam, C. G. T. 1984, *A&AS*, 58, 197
- Reich, W., Reich, P., & Fürst, E. 1990, *A&AS*, 83, 539
- Reynolds, S. P., & Moffett, D. A. 1993, *AJ*, 105, 2226
- Reynoso, E. M., Dubner, G. M., Goss, W. M., & Arnal, E. M. 1995, *AJ*, 110, 318
- Roberts, D. A., Goss, W. M., Kalberla, P. M. W., Herbstmeier, U., & Schwarz, U. J. 1993, *A&A*, 274, 427
- Roger, R. S., Milne, D. K., Kesteven, M. J., Wellington, K. J., & Haynes, R. F. 1988, *ApJ*, 322, 940
- Rosado, M. 1983, *RMxAA*, 8, 59
- Rosado, M., Ambrocio-Cruz, P., Le Coarer, E., & Marcelin, M. 1996, *A&A*, 315, 243
- Routledge, D., Dewdney, P. E., Landecker, T. L., & Vaneldik, J. F. 1991, *A&A*, 247, 529
- Saken, J. M., Fesen, R. A., & Shull, J. M. 1992, *ApJS*, 81, 715
- Sakhibov, F. Kh., & Smirnov, M. A. 1982, *SvAL*, 8, 150
- Sato, F. 1979, *Astrophys. Lett.*, 20, 43
- Schwarz, U. J., Goss, W. M., Kalberla, P. M., & Benaglia, P. 1995, *A&A*, 299, 193
- Seward, F. D., Dame, T. M., Fesen, R. A., & Aschenbach, B. 1995, *ApJ*, 449, 681
- Shaver, P. A., & Goss, W. M. 1970, *Aust. J. Phys. Supp.*, 14, 1
- Shklovsky 1960, *SvA*, 4, 243
- Stecker F. W., & Jones F. 1977, *ApJ*, 217, 843

- Tatematsu, K., Fukui, Y., Landecker, T. L., & Roger, R. S. 1990, *A&A*, 237, 189
- Taylor, A. R., Wallace, B. J., & Goss, W. M. 1992, *AJ*, 103, 931
- Thomas, B. MacA., & Day, G. A. 1969a, *Aust. J. Phys.*, 11, 1
- 1969b, *Aust. J. Phys.*, 11, 19
- Uchida, K., Morris, M., & Yusef-Zadeh, F. 1992, *AJ*, 104, 1533
- van den Bergh, S. 1988a, *ApJ*, 327, 156
- 1988b, *PASP*, 100, 205
- Whiteoak, J. B. Z., & Green, A. J. 1996, *A&AS*, 118, 329
- Wilner, D. J., Reynolds, S. P., & Moffett, D. A. 1998, *AJ*, 115, 247
- Winkler, F. P., & Long, K. S. 1997, *ApJ*, 491, 829